Efficient crystal structure prediction using universal neural network potential with diversity preservation in genetic algorithms

Takuya Shibayama,[1] Hideaki Imamura,[1] Katsuhiko Nishimra,[1] Kohei Shinohara,[1,*]
Chikashi Shinagawa,[1] So Takamoto,[1] and Ju Li[2]

[1]*Preferred Networks, Inc., Tokyo 100-0004, Japan*

[2]*Department of Nuclear Science and Engineering, and Department of Materials Science and Engineering, Massachusetts Institute of Technology, Cambridge, Massachusetts 02139, USA*

(Received 27 March 2025; revised 23 June 2025; accepted 11 May 2026; published 2 June 2026)

Crystal structure prediction (CSP) is crucial for identifying stable crystal structures in given systems and is a prerequisite for computational atomistic simulations. Recent advances in neural network potentials (NNPs) have reduced the computational cost of CSP. However, searching for stable crystal structures across the entire composition space in multicomponent systems remains a significant challenge. Here, we propose an improvement of a genetic algorithm (GA)-based CSP method using a universal NNP designed to efficiently expand convex hull volumes while preserving the diversity of crystal structures. Our hull-informed filtering and elitist-selection procedures incorporate an aging mechanism that prioritizes recently improved compositions. We also employ niching to prevent convergence to a small set of stoichiometries, thereby preserving a diverse, high-quality population. Our evaluation shows that the present method outperforms the symmetry-aware random structure generation and existing CSP methods, achieving a larger convex hull with fewer trials. We demonstrated that our approach, combined with the developed universal NNP (PFP), can accurately reproduce and explore phase diagrams obtained through DFT calculations; this indicates the validity of PFP across a wide range of crystal structures and element combinations. This study, which integrates a universal NNP with a GA-based CSP method, highlights the promise of these methods in materials discovery.

DOI: 10.1103/4knt-ccqg

I. INTRODUCTION

Computational atomistic simulations based on a quantum-mechanical description enhance our understanding of materials and even contribute to modern materials design [1]. Crystal structure prediction (CSP), a process to predict stable crystal structures in given systems, is a crucial prerequisite to harness the computational atomic simulations [2–5]. Despite the well-established methodology for analyzing crystal structures from experimental data, CSP is essential for accelerating materials discovery through the *ab initio* approach.

While CSP plays an integral role in predicting stable crystal structures, it represents a daunting global optimization task owing to the vast energy landscape. Substituting elements from known crystal structure prototypes is a prevailing method for generating candidate structures [6]. Although the prototype substitution method often gives reasonable results, its coverage falls short, especially in multicomponent systems. Metaheuristic algorithms offer another approach to creating novel crystal structures. These include methods such as random structure search [7], basin hopping [8], minima hopping [9,10], genetic algorithm (GA) [11–17], particle swarm optimization [18], and Bayesian optimization [19,20]. Typically, these CSP methods are combined with density functional theory (DFT) calculations to evaluate the formation energy of the candidate structures. However, the time-consuming DFT calculations, which limit the exploration of structures, significantly hinder the efficiency of CSP.

Recent advancements in machine learning potential, interatomic potential fitted by DFT calculations, enable an efficient approach to CSP thanks to their fast and accurate energy evaluation [21–25]. Because we are often interested in multicomponent systems like ternary or quaternary systems in CSP, it is preferable for the machine learning potential to exhibit scalability with the number of elements and transferability across various systems. Also, high accuracy is required to capture subtle energy differences among distinct structures in CSP. A universal neural network potential (NNP) trained with extensive datasets has been gaining significant attention owing to its scalability and transferability, which includes M3GNet [26,27], ALIGNN-FF [28], CHGNet [29], MACE-MP-0 [30,31], GNoME [32], Orb [33], EquiformerV2-OMat24 [34,35], MatterSim [36], and PFP [37–39].

Applying a machine learning potential to CSP is relatively straightforward, and it still achieves a significant improvement in efficiency [25,32,40–47]. Nevertheless, further development of CSP algorithms employing universal NNPs has room for enhancement. While the existing *ab initio* CSP methods

*Contact author: kshinohara@preferred.jp

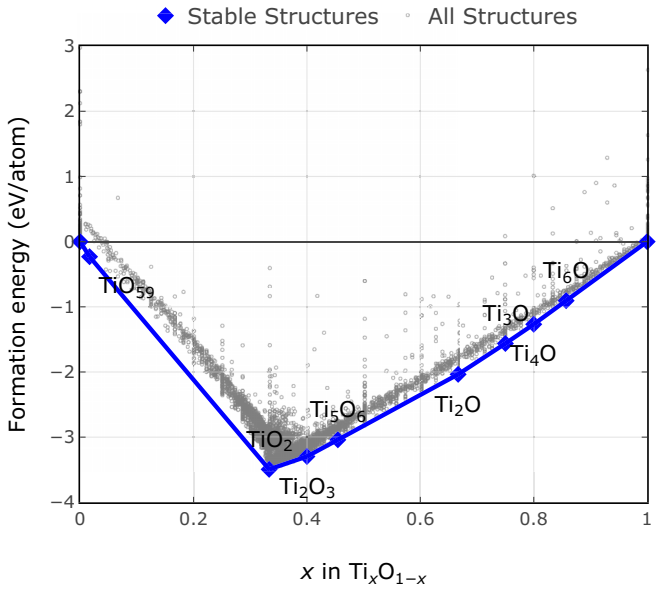

FIG. 1. Biased sampling of the convex hull in the Ti–O system by a standard GA-based CSP method.

often implicitly assume the number of energy evaluations to be limited due to the computational cost of DFT, the universal NNPs can allow us a vast number of energy evaluations and consider an entire convex hull concurrently, thereby appreciating the diversity of crystal structures all at once.

GA-based CSP methods exemplified by USPEX provide variable-composition searches and have enabled numerous discoveries [2,12,13,15]. However, they are not explicitly designed to optimize the entire convex hull. As a consequence, selection pressure and operator design tend to bias the search toward a few low-energy stoichiometries. Figure 1 illustrates this effect in the Ti–O system: when the composition is allowed to vary, a traditional GA-based CSP concentrates trials near TiO_2, leaving large regions of the hull insufficiently explored.

Recently, the convex hull genetic algorithm (CHGA) reframes variable-composition CSP as convex hull optimization, leveraging an analogy to Pareto-front optimization to act on the hull as a whole [48]. While promising, published validations have focused on two-element systems with on the order of 10^4 trials. In practice, exploring the entire convex hull requires much more massive simulations than composition-fixed searches. This becomes especially pronounced for ternary and higher-order systems, where 10^4 trials are insufficient to cover the hull. Moreover, as shown in Sec. IV, existing approaches often saturate early, slipping into local optima and thus failing to benefit from prolonged runs.

In this work, we propose a GA-based method that remains effective over long optimization by dynamically shifting the search region through controlled forgetting (aging) of outdated structures, while preserving diversity across populations (niching). Conceptually, our method stands on both traditional GA-based CSP and CHGA: (i) we adopt the GA pipeline with standard variation operators and the use of energy/hull information for ranking, and (ii) we explicitly shape the selection pressure at the level of the elitist selection so that the search does not collapse to a few stoichiometries during long optimization. Concretely, we (a) filter out unpromising trials using an age-weighted and hull-aware score, and (b) form the elite population by a hull-informed nondominated sorting coupled with niching tie-breakers.

The remainder of this paper is organized as follows. Section II describes PFP and a procedure for calculating formation energy with PFP in this study. Section III provides the problem setting and basic terminology, the background of GA-based CSP and CHGA, and the proposed method. Section IV shows the application of the present GA to a chemically diverse range of elements, from binary to octonary systems.

II. FORMATION ENERGY CALCULATION WITH PFP

A. PFP

In this study, we used our developed universal NNP called the PFP version 6.0.0 [38], which was trained on around 42 million structures. The PFP can be applied to arbitrary combinations of 72 supported elements (all elements from H to Bi except Tc, Pm, Eu, Tb, Dy, Ho, Er, Tm, Yb, Lu, and Tl). Its training dataset was collected with DFT calculations using plane-wave basis sets and the projector augmented wave (PAW) [49,50] with the Perdew–Burke–Ernzerhof (PBE) exchange-correlation functional [51] implemented in the Vienna *ab initio* simulation package (VASP) [52–54]. Details of the DFT calculations are described in Ref. [38].

For systems containing V, Cr, Mn, Fe, Co, Ni, Cu, Mo, or W, we prepared the DFT calculations with the generalized gradient approximation (GGA) with the PBE functional and GGA with Hubbard U corrections (GGA + U) introduced by Dudarev *et al.* [55]. The U-J parameters in GGA + U were adopted from the Materials Project (MP) [56] except for Cu and from Wang *et al.* [57] for Cu. We trained PFP simultaneously for the DFT calculations with and without Hubbard U corrections. The PFP has two modes to predict energies with and without Hubbard U corrections. We used PFP trained with Hubbard U corrections for oxides and fluorides containing V, Cr, Mn, Fe, Co, Ni, Cu, Mo, or W, and otherwise without Hubbard U corrections. This choice is consistent with MP except for Cu.

B. Reference simple systems

For formation energy calculations, we selected reference crystal structures for the 72 supported elements and 2 partially supported elements (Tc and Tl), as listed in Table I. For each element, we collected crystal structures from MP and searched for the lowest-energy structure after structural relaxation with PFP. The structural relaxation of atomic positions and lattice constants was performed until residual forces were less than 5×10^{-3} eV/Å. We matched the reference structures with the AFLOW standard encyclopedia of crystallographic prototypes [58] using `pymatgen` [59]. The third column of Table I displays the matched prototype structures within 0.1 meV/atom from the lowest-energy structure, which captures the diversity of stable prototype structures across various elements. The fourth column shows the PFP energy differences in meV/atom between two structures: one is the energy-lowest structure in PFP, and the other is the energy-lowest structure in DFT calculation in MP. While the

TABLE I. Reference simple systems for each element in this study. The second column shows initial structures for structural relaxation taken from MP, recorded with `material_id`. The third column shows prototype structures within 0.1 meV/atom from the lowest-energy structure. When a prototype is not found, `material_id` is denoted instead. The fourth column shows the PFP energy differences (meV/atom) between the present reference structures and the on-the-hull structures in MP.

H	mp-973783	β-O, mp-731827	4.3	Sr	mp-867202	A1 (fcc), A3 (hcp), A3' (α-La), C19 (α-Sm)	0.0
He	mp-614456	A1 (fcc), A3 (hcp)	0.8	Y	mp-112	A3 (hcp)	0.0
Li	mp-135	A2 (bcc)	0.7	Zr	mp-8635	A1 (fcc)	2.2
Be	mp-87	A3 (hcp)	0.0	Nb	mp-75	A2 (bcc)	0.0
B	mp-161	β-B	40.5	Mo	mp-129	A2 (bcc)	0.0
C	mp-568286	mp-568286, mp-990424	0.6	Tc	mp-113	A3 (hcp)	0.0
N	mp-570747	γ-N	5.7	Ru	mp-33	A3 (hcp)	0.0
O	mp-1180036	mp-1180036	41.3	Rh	mp-74	A1 (fcc)	0.0
F	mp-561203	A14 (molecular iodine)	0.0	Pd	mp-2	A1 (fcc)	0.0
Ne	mp-111	A1 (fcc)	0.0	Ag	mp-10597	A3 (hcp)	0.6
Na	mp-974920	A1 (fcc), A3 (hcp), A3' (α-La), C19 (α-Sm)	0.0	Cd	mp-94	A3 (hcp)	0.0
Mg	mp-1056702	A1 (fcc)	1.1	In	mp-973111	A3 (hcp)	1.9
Al	mp-134	A1 (fcc)	0.0	Sn	mp-117	A4 (diamond)	0.0
Si	mp-165	Lonsdaleite	5.9	Sb	mp-104	A7 (α-As)	0.0
P	mp-1198724	mp-1198724	9.6	Te	mp-567313	A8 (γ-Se)	0.0
S	mp-666931	mp-666931	0.7	I	mp-23153	A14 (molecular iodine)	0.0
Cl	mp-1008394	A14 (molecular iodine)	0.0	Xe	mp-570510	A1 (fcc), A3 (hcp), A3' (α-La), C19 (α-Sm)	0.0
Ar	mp-568145	A1 (fcc), A3 (hcp)	0.0	Cs	mp-639727	A1 (fcc), A3 (hcp), A3' (α-La)	0.0
K	mp-1184764	A1 (fcc), A3 (hcp), A3' (α-La), C19 (α-Sm)	0.0	Ba	mp-1096840	A2 (bcc)	0.0
Ca	mp-1183455	A1 (fcc), A3 (hcp), A3' (α-La)	0.0	La	mp-156	A1 (fcc), A3' (α-La)	0.0
Sc	mp-67	A3 (hcp)	0.0	Ce	mp-64	A20 (α-U)	5.4
Ti	mp-46	A3 (hcp)	16.5	Pr	mp-38	A1 (fcc), A3 (hcp), A3' (α-La), C19 (α-Sm)	0.0
V	mp-146	A2 (bcc)	0.0	Nd	mp-123	A1 (fcc), A3' (α-La), C19 (α-Sm)	0.0
Cr	mp-90	A2 (bcc)	0.0	Sm	mp-21377	A1 (fcc), A3 (hcp), A3' (α-La), C19 (α-Sm)	0.0
Mn	mp-35	A12 (α-Mn)	0.0	Gd	mp-155	A3 (hcp), C19 (α-Sm)	0.0
Fe	mp-1271068	A2 (bcc)	0.0	Hf	mp-103	A3 (hcp)	0.0
Co	mp-54	A3 (hcp)	6.0	Ta	mp-50	A2 (bcc)	29.6
Ni	mp-23	A1 (fcc)	0.0	W	mp-91	A2 (bcc)	0.0
Cu	mp-30	A1 (fcc)	0.0	Re	mp-8	A3 (hcp)	23.6
Zn	mp-1187812	A3 (hcp), C19 (α-Sm)	0.1	Os	mp-49	A3 (hcp)	0.0
Ga	mp-142	A11 (α-Ga)	0.0	Ir	mp-101	A1 (fcc)	0.0
Ge	mp-1007760	Lonsdaleite	4.1	Pt	mp-126	A1 (fcc)	0.0
As	mp-11	A7 (α-As)	23.0	Au	mp-1008634	A3 (hcp)	2.0
Se	mp-542605	mp-542605	1.1	Hg	mp-1184554	A3 (hcp), A3' (α-La), C19 (α-Sm)	2.4
Br	mp-1120813	mp-1120813	10.3	Tl	mp-151	A1 (fcc)	0.3
Kr	mp-976347	A1 (fcc), A3 (hcp), A3' (α-La), C19 (α-Sm)	0.0	Pb	mp-20745	A1 (fcc), A3 (hcp), A3' (α-La)	0.1
Rb	mp-12628	A1 (fcc), A3 (hcp), A3' (α-La), C19 (α-Sm)	12.8	Bi	mp-23152	A7 (α-As)	0.0

energy differences are particularly noticeable for layered or molecular crystal structures of B, O, As, and Br, possibly due to convergence issues in structural relaxations, PFP accurately evaluates stable crystal structures up to approximately 10 meV/atom.

C. MP compatibility and energy corrections

Because we used almost the same DFT settings as MP, we applied anion and GGA/GGA + U mixing scheme corrections [60] into PFP total energies for better predictions across diverse chemical systems. The policy regarding which modes of PFP to use with and without Hubbard U corrections in Sec. II A is compatible with the GGA/GGA + U mixing scheme in MP. The exception is an oxide with Cu, in which case we use a correction for Cu in Ref. [61]. Consequently, we can directly compare a convex hull with PFP and MP for all systems except oxides with Cu.

III. GA-BASED CSP METHOD

A. Problem setting and terminology

We consider CSP under variable compositions for a given list of elements [2,3]. Let M denote the number of elements, and let $r \in [0, 1]^M$ be a reduced composition with $\sum_{a=1}^{M} r_a = 1$. For a crystal structure i, let $r(i)$ be its reduced composition and $E(i)$ be its formation energy per atom after structural relaxation (Sec. II). Thermodynamic stability at 0 K is evaluated by the distance ("energy above hull") to the lower convex envelope of the energy–composition space; structures on the convex hull are thermodynamically stable with respect to decomposition into competing phases [62,63]. Our goal is to efficiently discover low-energy structures near or on the convex hull by exploring the joint space of compositions and periodic atomic configurations with up to a user-specified maximum number of atoms per unit cell. Throughout the paper, we assume that a list of elements (e.g., O–Sr–Ti) is given in advance, and the search spans all stoichiometries composed of those elements.

In this work, we adopt a *genetic algorithm (GA)* approach, which has achieved substantial success in CSP over the last two decades [2,3,11–17,48,64,65]. Our implementation improves the variable-composition *convex-hull genetic algorithm (CHGA)* paradigm [48] with convex hull aware optimization, particularly for improving performance in the case where $M > 2$.

We use standard GA terminology [2]. A *generation* is one cycle of variation and selection, and a *population* is the set of candidates in a generation. *Parents* are selected structures that produce *offspring* via variation operators. The variation operators that produce offspring from one or more parents are called *mutation* and *crossover*, respectively. *Selection* determines which candidates survive to the next generation; we use *elitist* selection to guarantee carryover of top performers and *niching* to maintain diversity across compositions and structures (e.g., fitness sharing [66], crowding-based schemes as in NSGA-II [67], or hyperplane-based methods in NSGA-III [68]). While not a term commonly used in genetic algorithm contexts, the term *trial* as employed in general iterative black-box optimization algorithms [69] refers to a pipeline of variation, structural relaxation, and formation energy evaluation for a single structure within a population.

The remainder of this section is organized as follows. In Sec. III B, we summarize the standard GA-based CSP pipeline exemplified by USPEX [2] (initialization, crossover/mutation, and fitness-based selection), and we briefly review a recent CHGA that explicitly casts variable-composition search as an optimization of the convex hull itself [48]. In Sec. III C, motivated by multicomponent systems ($M > 2$), we describe our hull-informed filtering and elitist selection procedures that integrate *aging* (to prefer recently improved compositions) and *niching* (to avoid collapse to a few stoichiometries), thereby maintaining a high-quality and diverse population across populations.

B. Background: Standard GA and convex-hull GA for CSP

1. Standard GA-based CSP

Figure 2 outlines a standard GA-based CSP method. After an initial population is produced by sampling, the algorithm

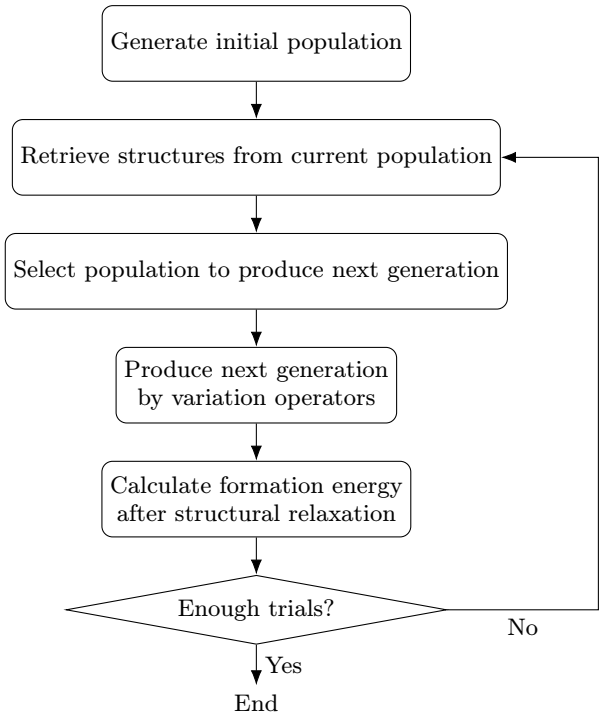

FIG. 2. Schematic diagram of the standard GA-based CSP method.

iterates until a sufficient number of trials have been completed: from each population, structures that should survive to the next generation and those that should serve as parents are selected; offspring are then created by applying variation operators to the selected parents, locally relaxed, and evaluated before the next iteration [2,13,15,16,70].

The initial population is commonly generated via random structure generation, which is also reused as a variation operator to maintain diversity [13,15,70]. Purely unconstrained random sampling tends to produce chemically similar, as the number of atoms per cell grows [71]. To mitigate this, existing methods split the simulation cell into multiple subcells, perform random sampling in a single subcell, and then copy it to the remaining subcells [71].

Because thermodynamically stable crystals often exhibit (partial) symmetry [7], symmetry-constrained generators are also employed at the subcell stage, in which atoms are assigned to compatible Wyckoff positions of a sampled space group. Popular software that implements these strategies includes `PyXtal` [72] and `AIRSS` [7].

Selection of survivors and parents to produce the next generation typically relies on a per-structure fitness value after local relaxation [2,3]. In GA-based CSP, this is commonly an energy-based criterion (e.g., formation energy or enthalpy per atom; lower is better), optionally augmented with similarity-aware penalties to avoid duplicates at the same stoichiometry [15,73–75]. To preserve diversity, deterministic truncation is often combined with stochastic schemes such as fitness-proportionate (roulette-wheel) selection [2].

Variation operators that produce offspring from one or more parents are called *mutation* and *crossover*, respectively; standard operators for periodic crystals include heredity

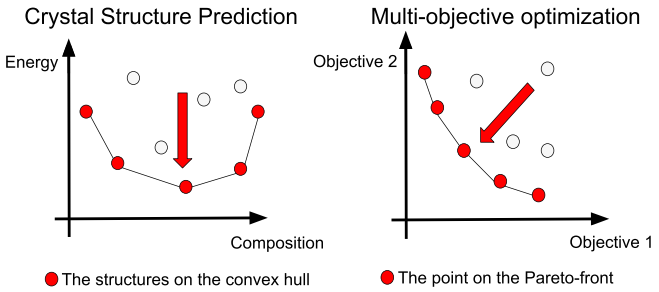

FIG. 3. The similarity between the convex hull in the energy-composition space and the Pareto front in the multiobjective optimization problem.

(cut-and-splice), lattice strain, atomic "rattle," and species permutation/transmutation [13–15,76].

2. Convex hull GA (CHGA)

CHGA reformulates variable-composition CSP as a direct *convex hull* optimization problem: instead of optimizing individual structures in isolation, the algorithm aims to optimize the hull itself, leveraging an analogy to Pareto-front optimization in multiobjective genetic algorithms [48]. Figure 3 illustrates the similarity between the convex hull in the energy-composition space and the Pareto front in multiobjective optimization.

In multiobjective optimization, NSGA-II/III [67,68] are widely used "gold standards": they apply nondominated sorting to partition a population into fronts and adopt elitist survival from lower-rank (better) fronts; niching then maintains diversity—via crowding distance in low dimensions (NSGA-II) or reference points on a hyperplane/simplex in higher dimensions (NSGA-III).

In CHGA, the dominance relation for nondominated sorting is defined via the convex hull [48]. For a given population, one first draws the convex hull in the energy-composition space and assigns *rank 0* to structures on the hull. Removing these and redrawing the hull yields *rank 1*, and repeating this "peeling" assigns a rank to every structure. Thus realizing a hull-based nondominated sort.

Survivor selection follows an elitist strategy analogous to NSGA families. As for tie-breaking, CHGA explores niching mechanisms tailored to hull optimization and reports, in two-element system tests (Li–Si), that niching was *not* critical; they instead used the convex hull hypervolume as a convergence indicator and recommended full elitism with a mix of bred and high-symmetry random generation [48].

C. Proposed method: Aging and niching for convex hull expansion

We propose a GA-based method that remains effective over long runs by dynamically shifting the search region through controlled forgetting (aging) of outdated structures, while preserving diversity across populations (niching). The difference from standard GA-based CSP and CHGA (Sec. III B) lies in the selection step (Fig. 2). Concretely, we (a) filter out unpromising trials using an age-weighted, hull-aware score (Sec. III C 1) and (b) form the elite population by a hull-informed nondominated sorting coupled with niching tie-breakers (Sec. III C 2). The overall workflow remains that of Fig. 2 and supports asynchronous trial evaluation.

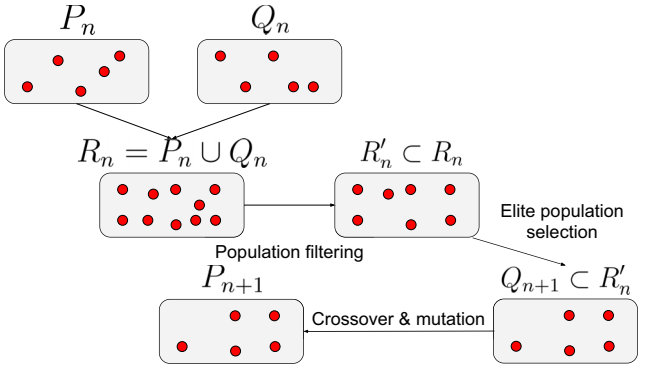

FIG. 4. The relationship between the parent population, elite population, filtered population, next elite population, and the next population.

1. Population filtering with aging and niching

The population filtering is performed to construct a subset of the parent population and the elite population. This step is just after retrieving the current population and before selecting the elite population, as shown in Fig. 2.

In this step, we selected structures close to the convex hull with the most recently updated composition. Our algorithm design is based on two intuitions: (1) lower-energy structures should exist near the structures close to the convex hull, and (2) there should be some room for improvement in the neighbors of the compositions that observed recent updates on their lowest energy. Population filtering is similar to the aging evolution strategy [77,78] in that it ignores the structures that have not been updated for a long time.

Let P_n be the parent generation, Q_n be the elite population used to select the parent generation, and $R_n = P_n \cup Q_n$, as shown in Fig. 4. Let $j_*(i)$ be the structure with the smallest energy in the neighborhood of the structure i defined as follows:

$$j_*(i) = \underset{j \in \bigcup_{k=1}^{n} P_k}{\operatorname{argmin}} \{E(j) \mid \|r(i), r(j)\|_1 < \delta\}, \tag{1}$$

where $\|x\|_1 = \sum_{k=1}^{d} |x_i|$ is the 1-norm, and $\delta > 0$ is the threshold of the 1-norm of the composition. Here, we use all the structures we have explored so far $\bigcup_{k=1}^{n} P_k$ as neighbors instead of R_n to maintain the diversity of the elite population. We define the distance to the convex hull of the structure i as

$$E(i) - E(j_*(i)). \tag{2}$$

Let $n^*(i)$ be the generation in which the structure $j_*(i)$ was generated. Let $E_{\max}$ and $E_{\min}$ be the maximum and minimum energies over all the structures explored so far defined as follows:

$$E_{\max} = \max \left\{ E(i) \mid i \in \bigcup_{k=1}^{n} P_k \right\},$$
$$E_{\min} = \min \left\{ E(i) \mid i \in \bigcup_{k=1}^{n} P_k \right\}. \tag{3}$$

We later normalize the distance to the convex hull $E(i) - E(j_*(i))$ to be between 0 and 1 by dividing it by $E_{\max} - E_{\min}$.

The population filtering is a procedure to construct a subset $R'_n \subset R_n$. For each element i in R_n, we calculated the following quantity by considering the distance to the convex hull $E(i) - E(j_*(i))$ (niching) and the generation difference $n - n^*(i)$ (aging):

$$D(i) = \frac{E(i) - E(j_*(i))}{E_{\max} - E_{\min}} \times \alpha^{n-n^*(i)}, \tag{4}$$

where $\alpha > 1$ is a tuning parameter. The parameter α controls the importance of the generation difference. The smaller $D(i)$ indicates that the structure is closer to the convex hull, and the composition has been updated more recently. We adopt only the structures i that satisfy $D(i) < \epsilon$, where ϵ is a tuning parameter. The parameter ϵ controls the threshold of the distance to the convex hull and the generation difference. Finally, we define the following set R'_n as the output of this step,

$$R'_n = \{i \in R_n \mid D(i) < \epsilon\}. \tag{5}$$

2. Niching to maintain diversity across the population

Niching is performed to construct the elite population Q_{n+1} from the filtered population R'_n. The elite population is used to select the parent population P_{n+1} for the next generation, as shown in Fig. 4. We can reduce computational costs and search for stable structures more efficiently by applying crossover and mutation only to promising structures.

While CHGA reported from binary-system benchmarks that explicit niching was unnecessary [48], our experiments on ternary and higher systems demonstrate that niching materially improves hull coverage and prevents collapse to a few stoichiometries (see Sec. IV). Accordingly, we retain convex hull-based nondominated sorting for elitist selection, but for tie-breaking within the same hull layer, we adopt niching mechanisms inspired by NSGA-II/III [48,67,68] and adapt them to the energy-composition geometry of CSP, thereby maintaining diversity across the population. We observed that the NSGA-III-like niching procedure outperformed the NSGA-II-like one in our preliminary experiments, consistent with the general trend that NSGA-III is more effective in higher systems.

First, we define a procedure using the crowding distance similar to NSGA-II. The definition of crowding distance is different because we consider a different problem from the usual multiobjective optimization problem.

Let $H^{(k,a)}$ be the set of H^k, the output of the population filtering with rank k, sorted by $r(i)_a$. For each $a \in \{1, \ldots, M\}$ and structure i, let $r(i)_{a,\text{left}}$ and $r(i)_{a,\text{right}}$ be the ratio of the ath element in the structures on both sides of i in $H^{(k,a)}$, and let $\Delta_r(i,a)$ be the difference between them,

$$\Delta_r(i,a) = r(i)_{a,\text{right}} - r(i)_{a,\text{left}}. \tag{6}$$

Similarly, for the energy $E(i)$, let $H^{(k,E)}$ be the set of H^k sorted by $E(i)$. For each structure i, let $E(i)_{\text{right}}$ and $E(i)_{\text{left}}$ be the energies of the structures on both sides of i in $H^{(k,E)}$ and $\Delta_E(i)$ be the difference of them as follows:

$$\Delta_E(i) = E(i)_{\text{right}} - E(i)_{\text{left}}. \tag{7}$$

ALGORITHM 1. NSGA-II inspired niching.

Require: Population set H^k with rank k, number of selected structures ℓ
Ensure: Set $\hat{H}^k$ containing ℓ structures with smallest $c(i)$
for each $a \in \{1, \ldots, M\}$ **do**
  Sort H^k by $r(i)_a$ to create $H^{(k,a)}$
  for each structure $i \in H^k$ **do**
    Identify neighboring structures in $H^{(k,a)}$
    Compute $r(i)_{a,\text{left}}$ and $r(i)_{a,\text{right}}$
    Compute $\Delta_r(i,a) = r(i)_{a,\text{right}} - r(i)_{a,\text{left}}$
  end for
end for
Sort H^k by energy $E(i)$ to create $H^{(k,E)}$
for each structure $i \in H^k$ **do**
    Identify neighboring structures in $H^{(k,E)}$
    Compute $E(i)_{\text{left}}$ and $E(i)_{\text{right}}$
    Compute $\Delta_E(i) = E(i)_{\text{right}} - E(i)_{\text{left}}$
end for
for each structure $i \in H^k$ **do**
    Compute crowding distance:

$$c(i) = \Delta_E(i) \times \sum_{a=1}^{M} \Delta_r(i,a)$$

end for
Sort structures in H^k by $c(i)$ in ascending order
Select the first ℓ structures with the smallest $c(i)$ to form $\hat{H}^k$
return $\hat{H}^k$

Note that the energy of each structure is min-max normalized for stability.

Using the $\Delta_r(i,a)$ and $\Delta_E(i)$ defined above, we define the crowding distance $c(i)$ for the structures i in H^k as follows:

$$c(i) = \Delta_E(i) \times \sum_{a=1}^{M} \Delta_r(i,a). \tag{8}$$

We can order structures with the same rank by selecting structures with small crowding distance $c(i)$. The algorithm is summarized in Algorithm 1.

Next, we define the hyperplane-based method similar to NSGA-III. To clarify the method, we need to define reference points and how to measure distances. We adopt the following distance:

$$d(i,j) = |E(i) - E(j)| \times \sum_{a=1}^{M} |r(i)_a - r(j)_a|. \tag{9}$$

We constructed the reference points as follows. For each composition axis $a \in \{1, \ldots, M\}$, select the structure with the maximum $r(i)_a$ in H^k and call them $i_1, \ldots, i_M$. Then, consider an $(M-1)$-dimensional simplex with $i_1, \ldots, i_M$ as vertices, and place points $r_1, \ldots, r_K$ uniformly at regular intervals on it, and use these as reference points. Here, K is determined by the number of points to be placed on the edge of the $(M-1)$-dimensional simplex, and if $k+1$ points are placed on the edge, $K = \binom{M+k-1}{k}$. The algorithm is summarized in Algorithm 2.

ALGORITHM 2. NSGA-III inspired niching.

Require: Population set H^k with rank k, number of selected structures ℓ
Ensure: Set $\hat{H}^k$ containing ℓ structures distributed along the reference lines
Normalize each objective variable to be non-negative
Construct reference lines:
Define K reference points by selecting structures $i_1, \ldots, i_M$ with maximum $r(i)_a$ for each axis $a \in \{1, \ldots, M\}$
Place K points $r_1, \ldots, r_K$ uniformly on an $(M-1)$-dimensional simplex
for each structure $i \in H^k$ **do**
    for each reference line j **do**
        Project i onto reference line j
        Compute distance $d(i, j) = |E(i) - E(j)| \times \sum_{a=1}^{M} |r(i)_a - r(j)_a|$
    end for
    Assign i to the reference line j^* with the smallest $d(i, j)$
    Add i to the neighborhood set of j^*
end for
while size of $\hat{H}^k$ is less than ℓ **do**
    Select reference line j^* with the smallest neighborhood set
    Select structure i^* in the neighborhood set of j^* closest to the reference line
    Add i^* to $\hat{H}^k$ and remove it from the neighborhood set of j^*
end while
return $\hat{H}^k$

3. Other implementation details

Local relaxation. For the next population, the formation energy is calculated after structural relaxation with PFP [37–39], as described in Sec. II.

Asynchronous parallelization. Note that we present the workflow in Fig. 2 with clarity, assuming a synchronous search per generation. In practice, each trial can be evaluated asynchronously for high parallelism; once a structure returns, its parent generation is retrieved (by its generation index), and selection data structures are updated. Such trial-level asynchrony is naturally supported by modern optimization frameworks such as `Optuna` [69].

`PyXtal`*-based random structure generation.* We use symmetry-aware random structure generation by `PyXtal` [72] for the random structure generation in the sub-cells, thereby improving the search efficiency because stable crystal structures tend to have high symmetry [7]. The random structure generation by `PyXtal` requires a composition and a space-group type as input. We sampled the number of atoms in the unit cell uniformly up to the given maximum number of atoms in the unit cell and selected a composition from a multinomial distribution where each element has an equal probability. We sampled a space-group type uniformly from all space-group types other than $P1$. As some combinations of a composition and a space-group type are infeasible to generate a crystal structure, we retried the entire sampling process until a crystal structure is successfully generated.

Variation operators. Crossover and mutation are the processes of generating new structures P_{n+1} from the elite population Q_{n+1}. Crossover involves combining two parent structures to generate a child structure, and mutation involves changing the structure of a parent structure. The crossover and mutations used in our proposed method are listed in Table II. Several methods are implemented in `ASE` [70], and we modify some of the implementations [79].

The cut-and-splice crossover is a method to generate a child structure by cutting two parent structures at their unit cells along a crystal plane and joining them [11,80]. Because its implementation in ASE only allowed crossover between parent structures with the same composition, we modify it to allow crossover between parent structures with different compositions, which is already known in the field of CSP [14,76].

The random atom deletion mutation is a method to generate a child structure by randomly removing one atom from the parent structure. This mutation is effective to change the composition of the structure and t explore the composition space.

USPEX and CHGA can use random structure generation for a fixed number of trials to maintain the diversity of the composition in the population [2,48], but our proposed method incorporates it as a standard mutation operation. The random structure generation mutation is a method to generate a child structure by the random structure generation by `PyXtal`. This mutation can effectively maintain the diversity of the composition in the population.

TABLE II. Crossover and mutation methods used in the proposed GA-based CSP method.

Method	Description	Selection probability
Cut-and-splice crossover	Generate a child structure by cutting two parent structures at their unit cells along a crystal plane and joining them [14,76].	1/2
Random composition mutation	Generate a child structure by randomly changing its composition [13,15,76].	1/12
Strain mutation	Distort the unit cell by applying a random strain matrix to the basis vectors [13,15,76].	1/12
Rattle mutation	Perturb the atomic positions by a random displacement [13,15,76].	1/12
Permutation mutation	Swap the atomic positions of two selected atoms [13,15,76].	1/12
Random atom deletion mutation	Generate a child structure by randomly removing one atom from the parent structure.	1/12
Random structure generation mutation	Generate a structure by the random structure generation [48].	1/12

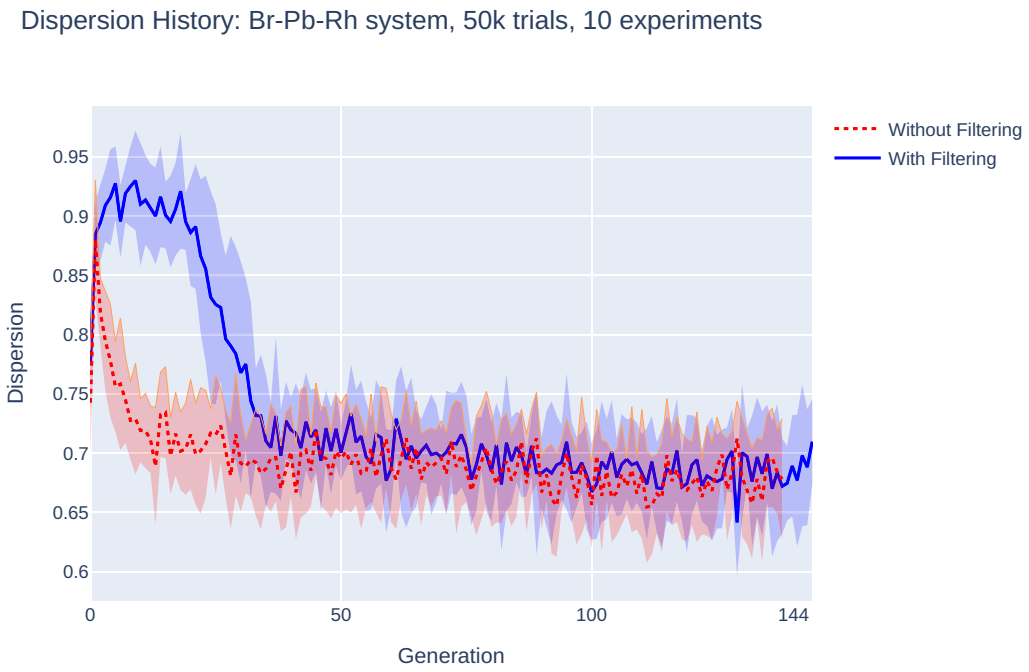

FIG. 5. Compositional dispersion history of the Br–Pb–Rh system. The Average Nearest Neighbor Index (ANNI) is plotted against the generation number. The blue line indicates the case with population filtering, while the red line indicates the case without population filtering. The shaded area represents the standard deviation of ANNI values across ten experiments. Lower ANNI values indicate greater compositional skewness.

IV. RESULTS AND DISCUSSION

In this section, we present the results of our proposed method for CSP using PFP and GA. First, we conducted an ablation study of the population filtering in Sec. IV A to demonstrate the effectiveness of the half of the proposed method. Secondly, we conducted an ablation study of the niching methods in Sec. IV B to demonstrate the effectiveness of the other half of the proposed method. Thirdly, we evaluated the performance of the proposed method by comparing it with existing methods in Sec. IV C. We then demonstrated the effectiveness of the proposed method by performing CSP searches for binary and ternary systems with MP in Sec. IV D. The results demonstrate that the proposed method can efficiently explore the search space and discover new crystal structure candidates that update the convex hull of MP. For the energy evaluation, we used the energy corrections described in Sec. II C.

A. Ablation study of population filtering

In this section, we conducted an ablation study of the population filtering. Population filtering is performed immediately prior to elitist selection in each generation to preserve the diversity of candidate compositions. The ablation study compared two cases: one with population filtering and one without. We demonstrated that implementing population filtering enables exploration of a wider range of structures across various compositions compared to its absence.

In this experiment, we examined the Br–Pb–Rh system with the following parameters: maximum number of atoms in the unit cell was 128, the population size was 250, the total number of trials was 50 000, $\alpha = 2.4$, and $\epsilon = 0.25$. We repeated the search 10 times for each case to account for the stochastic nature of the CSP search. The genetic operations and their selection probabilities are specified in Table II. We conducted comparisons under two conditions: with and without enabling population filtering as described in Sec. III C 1.

To quantitatively assess how compositional dispersion evolves across generations, we employed the Average Nearest Neighbor Index (ANNI) [81] to evaluate the compositional homogeneity of structures explored in each generation. Lower ANNI values indicate greater compositional skewness, which implies that the explored structures are concentrated in a narrower compositional range. On the other hand, higher ANNI values indicate a more diverse distribution of compositions. As shown in Fig. 5, when population filtering is enabled, the ANNI values are significantly higher during early generations compared to when filtering is disabled, indicating greater compositional dispersion. However, beginning approximately from the 40th generation onward, ANNI values become comparable regardless of whether population filtering is active or not, suggesting that compositional distribution becomes similarly skewed throughout both search phases.

Figure 6 illustrates the distribution of compositions of structures explored at each generation for one search. At generations 5 and 25, we observe that enabling population filtering results in a more broadly distributed range of structural compositions. From generation 50 onward, even when population filtering is active, the distribution of compositions becomes narrower, exhibiting patterns similar to when population filtering is disabled. Conversely, when population filtering is disabled, the explored structures show concentration within a narrow compositional range, and

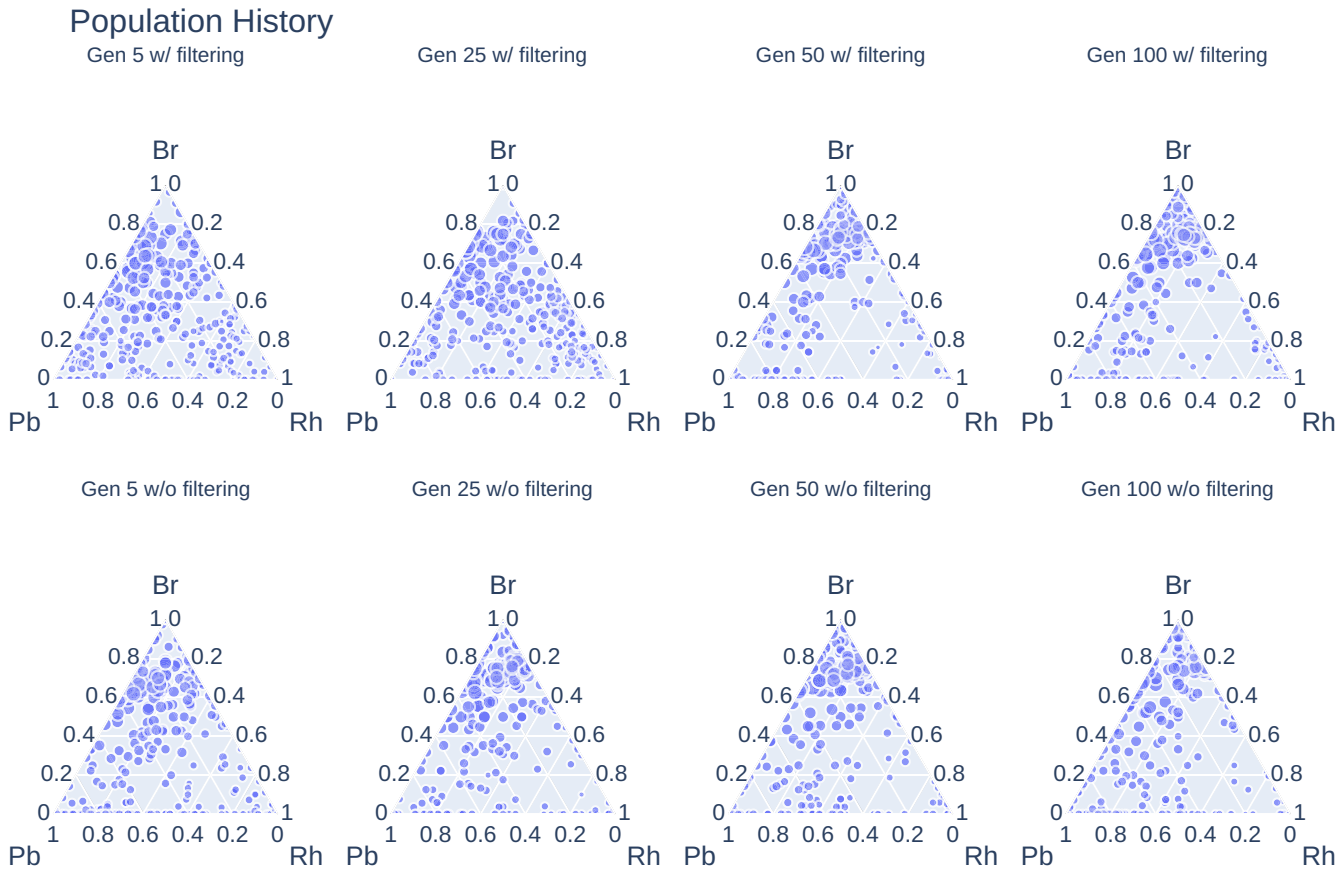

FIG. 6. Compositional distribution of structures explored at each generation in the Br–Pb–Rh system. The upper panel shows the case with population filtering, while the lower panel shows the case without population filtering. From left to right, the generations are 5, 25, 50, and 100. Each point represents a structure in the population; the point size is proportional to the absolute value of the formation energy. With filtering, the population is broadly dispersed across compositions in early generations and gradually concentrates on promising stoichiometries in later generations. Without filtering, the compositional distribution remains narrowly concentrated throughout all generations.

this range remains relatively stable across generations. This demonstrates that population filtering enables exploration of structures across a wider portion of the search space.

B. Ablation study of niching methods

In this section, we present the results of an ablation study conducted to evaluate the impact of different niching methods on search performance. Here, niching refers to the techniques employed during elite population selection in each generation, as described in Sec. III C 2, to maintain diversity across the population.

We compared the proposed NSGA-II and NSGA-III based niching methods with a no-niching method and an existing hypervolume contribution-based niching method [48]. Additionally, considering that previous studies [48] suggest that niching has a minor impact on search performance, we also included an ensembled method that randomly selects one of the niching methods for each trial to enhance search performance. To evaluate the influence of different element systems, we conducted experiments on three ternary systems: O–Sr–V, Br–Pb–Rh, and Li–Pr–Te. The search conditions were the same as those in Sec. IV A.

Figure 7 shows the result of search performance for each niching method, evaluated by hull volume following Ref. [48]. For average performance, the best methods were HV Contribution, No Niching, and NSGA-II for O–Sr–V, Br–Pb–Rh, and Li–Pr–Te, respectively. However, most methods fell within ± 1 standard deviation, indicating that the performance differences were not particularly significant. Although performance differences vary by element system, the ensembled method generally demonstrates the highest search performance. This suggests that different niching methods explore varying diversities of structures, and by ensembling them, a broader range of structures can be explored, leading to improved search performance.

C. Quantitative comparison with existing methods and MP

We quantitatively evaluated the proposed method compared with the symmetry-aware random search implemented in `PyXtal` [72], the traditional GA-based method implemented in `ASE` [70], and CHGA [48]. In this experiment, we fixed the following inputs and parameters: the maximum number of atoms in the unit cell was 128, the population size was 250, the total number of trials was 50 000, and $\alpha = 2.4$, $\epsilon = 0.25$. The genetic operations and their selection probabili-

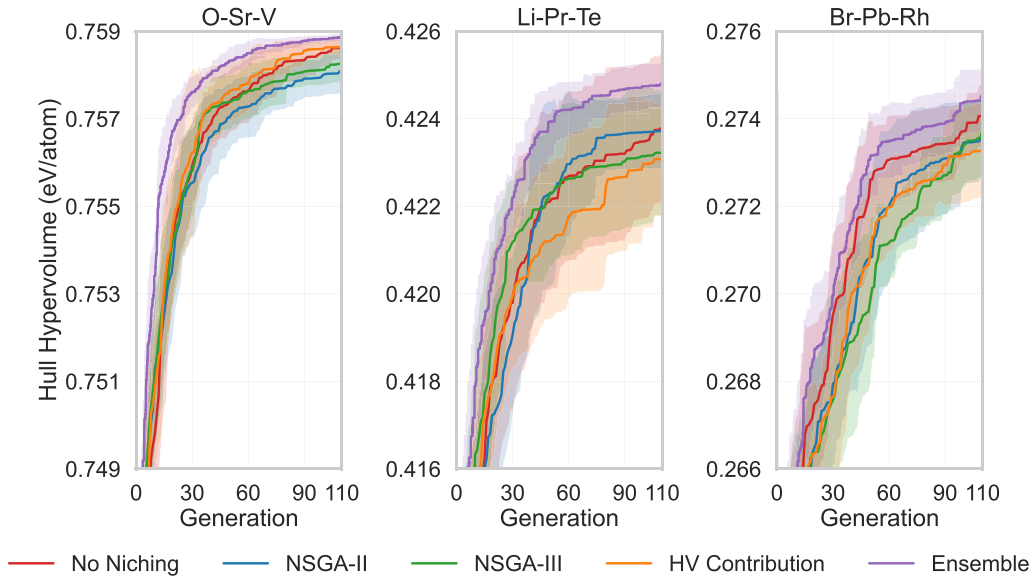

FIG. 7. Comparison of hull volume history for different niching methods in (left) O–Sr–V, (middle) Br–Pb–Rh, and (right) Li–Pr–Te systems. The no-niching method (red), the proposed NSGA-II based method (blue), the proposed NSGA-III based method (green), the existing hypervolume contribution-based method (orange), and the ensembled method (purple) are compared. Solid lines indicate the mean hull volume across repeated searches, and shaded regions indicate the standard deviation.

ties are listed in Table II. We chose four systems ranging from ternary to octonary systems: O–Sr–Ti and Ba–Ca–Cu–O–Tl as well known oxide systems [82], and Cu–Ga–Rh–Sc and Co–Cr–Cu–Fe–Mn–Ni–Ti–V as random alloy systems. The Hubbard U correction for Cu is applied for our method, while it is not applied for MP, which may affect the comparison in the Ba–Ca–Cu–O–Tl system, as mentioned in Sec. II A.

We evaluated each search by the volume of the convex hull, which can assess both the depth of the convex hull and the diversity of the included structures [48]. The hull volume value of the M-element system is normalized by the unit hull volume $V_{\mathrm{unit},M} = 1\,\mathrm{eV}/M!$, which corresponds to the volume of the convex hull with only one crystal structure on the hull with formation energy of -1 eV/atom. We performed the search by five times for each system because the CSP search involves randomness. Additionally, we compared the hull volume with that of MP. We performed structure optimization by PFP for MP structures within 0.2 eV/atom in MP convex hull to construct the MP convex hull. The absolute value of the hull volume depends on the element system and cannot be compared across different systems.

Figure 8 illustrates how the hull volume changed as the search progressed for each system, indicating that the proposed method outperformed random search for all the element systems. The final mean hull volumes for each system are listed in Table III. Here, we denote the mean hull volume of the proposed method as V_{proposed}, and that of the random search as V_{random}. The improvements of final mean hull volumes of the proposed method compared with random search are 0.014, 0.014, 0.027, and 0.024 for O–Sr–Ti, Cu–Ga–Rh–Sc, Ba–Ca–Cu–O–Tl, and Co–Cr–Cu–Fe–Mn–Ni–Ti–V, respectively. These improvements correspond to updates of the convex hull by 14 to 27 meV/atom if only one entry exists on the convex hull. We mention that the conversion of a hull volume to a formation energy update depends on the shape of the convex hull.

The proposed method also outperformed the original CHGA for all the element systems, as shown in Fig. 8. The difference in performance varies qualitatively depending on the element system. For the ternary system of O–Sr–Ti, both methods achieved similar hull volumes, but the proposed method outperformed the original CHGA in the early generations. For the quaternary system of Cu–Ga–Rh–Sc, the proposed method consistently outperformed the original CHGA throughout the search, especially in the early generations. For the quinary system of Ba–Ca–Cu–O–Tl, both methods achieved similar hull volumes at the early generations, but the proposed method outperformed the original CHGA in the later generations. For the octonary system of Co–Cr–Cu–Fe–Mn–Ni–Ti–V, the proposed method significantly outperformed the original CHGA at early generations, while both methods achieved similar hull volumes in the later generations. These results indicate that the proposed method can efficiently explore the search space faster than CHGA, especially in multicomponent systems. The final mean hull volumes for each system are listed in Table III. We denote the mean hull volume of CHGA as V_{chga}. The improvements of final mean hull volumes of the proposed method compared with CHGA are 0.002, 0.005, 0.014, and 0.0 for O–Sr–Ti, Cu–Ga–Rh–Sc, Ba–Ca–Cu–O–Tl, and Co–Cr–Cu–Fe–Mn–Ni–Ti–V, respectively.

The updated hull volume by the proposed method compared with that of MP is 0.023, 0.049, –0.016, and 0.031 for O–Sr–Ti, Cu–Ga–Rh–Sc, Ba–Ca–Cu–O–Tl, and Co–Cr–Cu–Fe–Mn–Ni–Ti–V, respectively; this corresponds to 0.5, 2.4, –0.3, and 2.0% of MP hull volume, respectively. The proposed method achieved larger convex hull volumes than MP for systems except for the Ba–Ca–Cu–O–Tl.

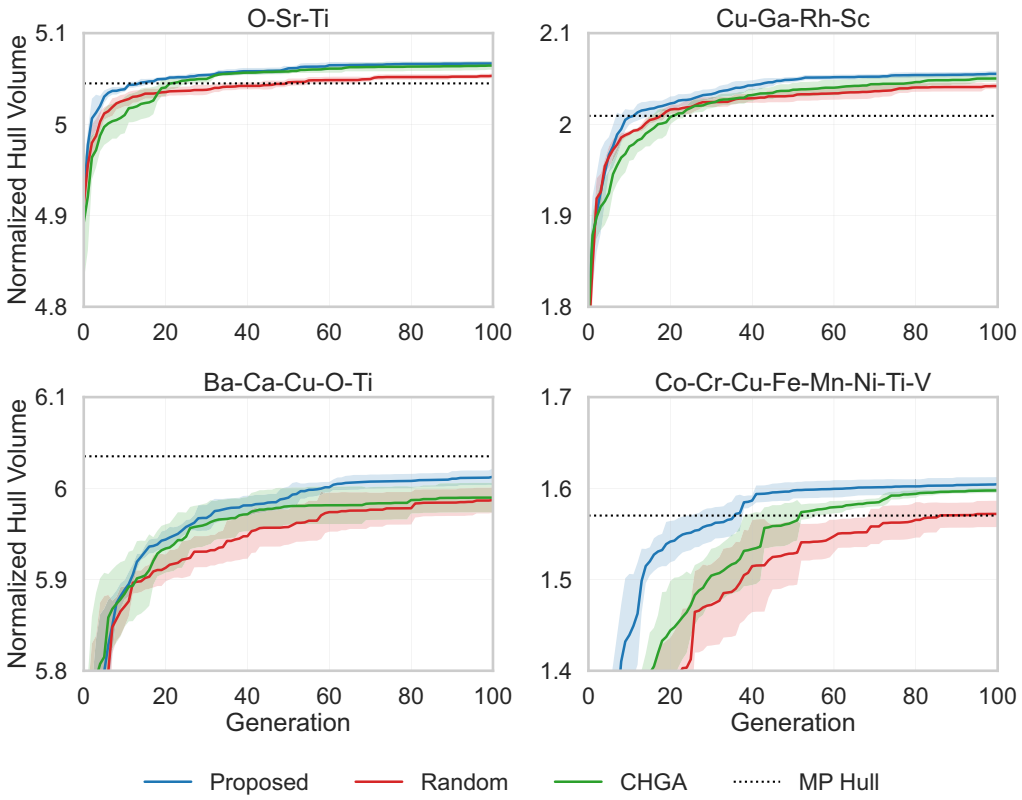

FIG. 8. Comparison between random search (red), CHGA (green), and the proposed method (blue) by the hull volume history. Solid lines indicate the mean hull volume across five experiments, and shaded regions indicate the standard deviation. The black dashed line indicates the normalized volumes for the convex hull constructed from MP structures.

Figure 8 also depicts the efficiency of the CSP search with the proposed method. The number of generations required to reach 99% of each final hull volume for O–Sr–Ti, Cu–Ga–Rh–Sc, Ba–Ca–Cu–O–Tl, and Co–Cr–Cu–Fe–Mn–Ni–Ti–V were 4, 34, 26, and 641, respectively, for the proposed method, 5, 28, 33, and 72, respectively, for a random search, and 11, 41, 20, 71, respectively, for CHGA; this indicates that the proposed method can efficiently explore the search space, especially in multicomponent systems.

We validated the effectiveness of our proposed method for actual applications by comparing the convex hulls of CSP and that of MP. Table III shows the average number of MP structures below, around, and above the convex hull of CSP searches. The structures around the hull are defined as those with energy above hull within 0.01 eV/atom. The structures below and above the hull are those with energy above hull less than -0.01 eV/atom and greater than 0.01 eV/atom, respectively. The average ratio of the number of MP structures around and above the convex hull to the total number of structures is 1.00, 0.88, 0.80, and 0.85 for O–Sr–Ti, Cu–Ga–Rh–Sc, Ba–Ca–Cu–O–Tl, and Co–Cr–Cu–Fe–Mn–Ni–Ti–V, respectively. Although the trends vary by element systems, around 80% of MP structures are reproduced by CSP. In particular, all MP structures are reproduced in the O–Sr–Ti system.

D. CSP for binary and ternary systems

We demonstrated the capability of our CSP method using PFP to discover new crystal structure candidates for binary

TABLE III. Mean normalized hull volume and average number of MP hull structures compared with our CSP hull. The second column shows the mean normalized hull volume of the proposed method, while the last three columns show that for the random search, CHGA, and the normalized hull volume of MP, respectively. The third to fifth columns show the average number of MP structures below, around, and above the CSP hull by the proposed method, respectively (see the main text for the detailed definition). The sixth column shows the average ratio of the number of MP structures around or above the CSP hull.

System	V_{proposed}	Below hull	Around hull	Above hull	Reproducibility	V_{random}	V_{chga}	V_{MP}
O–Sr–Ti	5.068	0	12.0	6.0	1.00	5.054	5.066	5.045
Cu–Ga–Rh–Sc	2.058	3.0	17.2	4.8	0.88	2.044	2.053	2.009
Ba–Ca–Cu–O–Tl	6.019	10.0	29.8	11.2	0.80	5.992	5.992	6.035
Co–Cr–Cu–Fe–Mn–Ni–Ti–V	1.601	8.4	38.4	10.2	0.85	1.577	1.601	1.570

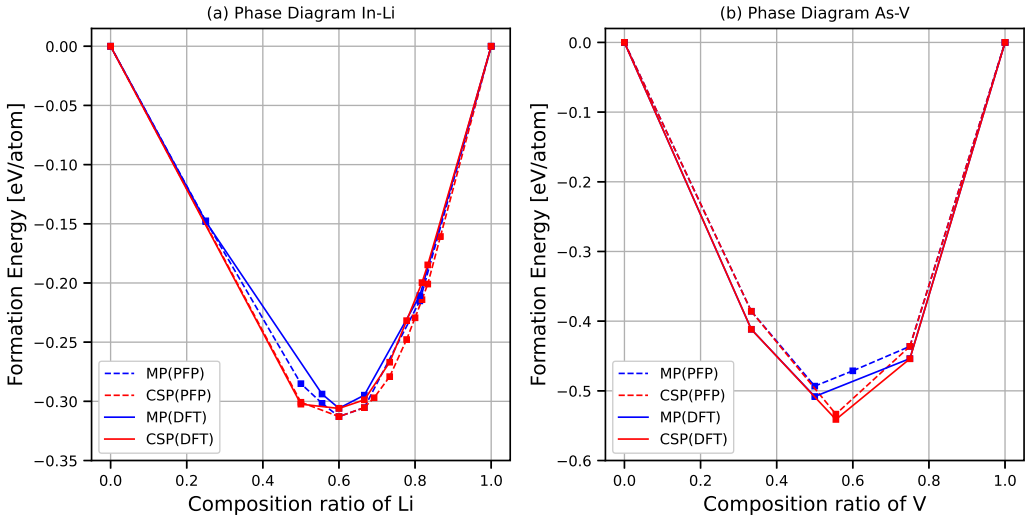

FIG. 9. Binary phase diagrams of (a) In–Li and (b) As–V systems. Red and blue lines show the convex hulls of the formation energy of our CSP results and MP, respectively. The energy is evaluated by VASP for solid lines, while PFP is used for dashed lines.

and ternary systems. The search conditions were the same as those in Sec. IV C; however, the structures from MP were added to the initial population of the search. The crystal structures obtained from the search were re-evaluated using DFT calculations to verify their validity. We report the results for systems In–Li, As–V, Al–Li–Pd, and La–Mo–O shown in Figs. 9 and 10.

Figure 9 depicts the convex hulls by our CSP methods and MP, respectively. DFT calculations with VASP were performed for these structures using the same settings as in Sec. II A. By comparing convex hulls, the structures identified through our CSP method are confirmed to be also stable in DFT calculations. These findings suggest that the CSP approach using PFP is highly effective in discovering new crystal structure candidates.

Figure 10 shows comparisons of MP and CSP phase diagrams for ternary systems. Numerous promising new crystal candidates have also been discovered in the ternary systems. Our CSP methodology demonstrates the ability to explore and update the entire phase diagram comprehensively.

Crystal structures that update the convex hull of MP in the systems shown in Figs. 9 and 10 are listed in Table IV [83]. The space-group type was identified using `spglib` with `symprec = 0.01` and `angle_tolerance = 5` [84]. Additionally, we matched these crystal structures with AFLOW prototypes [58,85–87] by assigning the AFLOW label using `aviary.wren` [88]. Several crystal structures were not found as prototype structures in the AFLOW database, indicating that our CSP method can discover novel crystal structures. Some of the listed crystal structures are visualized in Fig. 11.

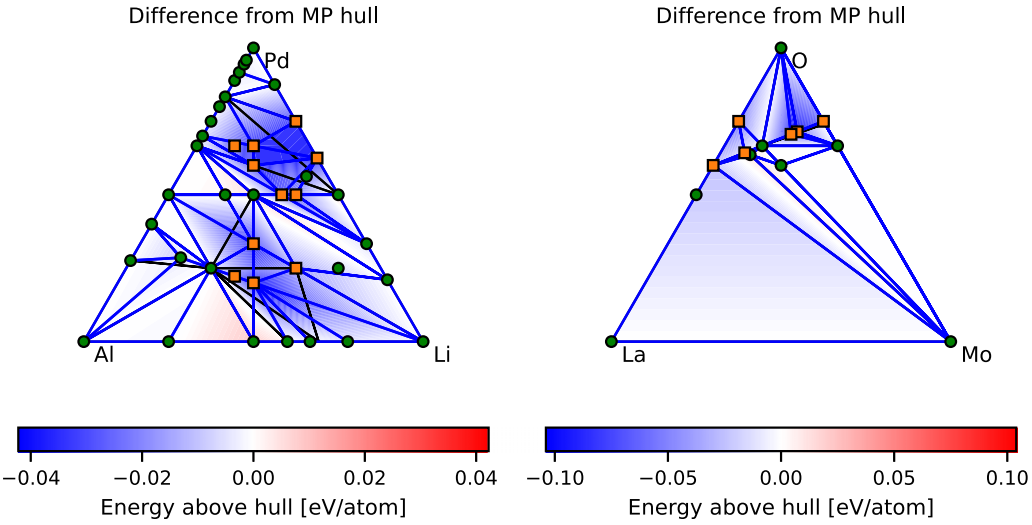

FIG. 10. Phase diagrams of ternary systems. Black and blue lines show the convex hulls of MP and our CSP results, respectively. Here, formation energies were evaluated with DFT calculations. Blue and red hatchings indicate the differences between the MP and our CSP convex hulls. The blue region shows the CSP results updating the MP convex hull. Markers display the simplices of the CSP convex hull, while orange squares indicate those with energy updates greater than 10 meV/atom.

TABLE IV. List of crystal structures that update the convex hull. The fourth column shows the matched AFLOW prototype if it exists.

Formula	Space-group type	Hull energy update [meV/atom]	AFLOW prototype
In_2Li_2	$Pmma$	−35	AB_oP4_51_e_f-001
In_2Li_7	$P\bar{1}$	−1	
In_4Li_{11}	$P\bar{1}$	−10	
In_4Li_9	$C2/m$	−5	
As_4V_5	$I4/m$	−45	A4B5_tI18_87_h_ah-001
Al_2Li_2Pd	$C2/m$	−42	
$Al_2Li_2Pd_2$	$P\bar{3}m1$	−34	
$Al_2Li_2Pd_6$	$P2_1/m$	−33	
$Al_2Li_4Pd_2$	$P4_2/mmc$	−14	
$Al_2Li_4Pd_6$	$P2_1/m$	−25	
$Al_2Li_6Pd_8$	$Im\bar{3}m$	−19	
Al_2Li_7	$P\bar{1}$	−4	
Al_2LiPd_6	$P\bar{1}$	−18	
Al_3Pd_7	$C2/m$	−4	
$Al_4Li_3Pd_2$	$P\bar{3}m1$	−22	
Al_4LiPd_2	$P\bar{1}$	−8	
$AlLi_5Pd_2$	$P\bar{4}m2$	−4	
$AlLiPd_4$	$Cmmm$	−33	
$AlPd_{11}$	$Cmmm$	−3	
$AlPd_{17}$	$P4/mmm$	−1	
$Li_{33}Pd_{55}$	$P\bar{1}$	−36	
$LiPd_3$	$Cmmm$	−33	AB3_oC8_65_a_bf-001
La_2O_6	$C2/m$	−58	
$La_2Mo_2O_6$	$R3c$	−1	
$La_2Mo_4O_{15}$	$P\bar{1}$	−100	
$La_4Mo_6O_{24}$	$P\bar{1}$	−105	
La_4MoO_9	$C2$	−12	
Mo_3O_9	Cm	−60	

V. CONCLUSION

We have presented the efficient GA-based CSP method using our developed universal NNP, PFP. Our method comprehensively explores the entire composition space and successfully discovers numerous stable crystal structures. The proposed method even identified unregistered stable crystal structures in MP, and subsequent DFT calculations validated their stability. Given that CSP requires precise formation energy accuracy to distinguish various polymorphs, these results also demonstrate the validity of PFP for a wide range of crystal structures and element combinations. To efficiently search the entire composition space, we have proposed the novel elitist selection method inspired by multiobjective optimization techniques, which considers both formation energies and compositions. Since the proposed GA-based CSP method is agnostic to how to generate initial populations, it would be fruitful in future works to combine it with other structure generation methods to tackle the vast search spaces in CSP, such as generative models for crystal structures. Our present method and results show significant promise for accelerating materials discovery.

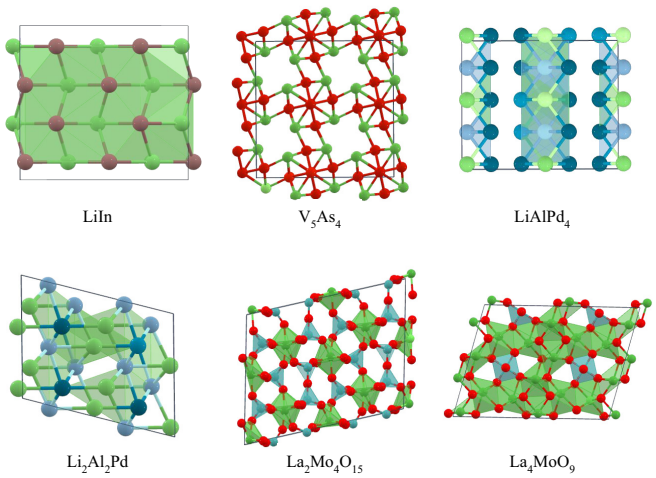

FIG. 11. Crystal structures that update the convex hull.

ACKNOWLEDGMENTS

We would like to thank our colleagues from Preferred Networks, Inc. for helpful discussions and support, including Shuhei Watanabe. PFP v6 was developed using the National Institute of Advanced Industrial Science and Technology's AI Bridging Cloud Infrastructure (ABCI) in addition to in-house supercomputers in Preferred Networks, Inc.

T.S., H.I., K.N., K.S., C.S., and S.T. are employees of Preferred Networks, Inc. Matlantis Corp., a joint venture among Preferred Networks Inc., ENEOS Corporation, and Mitsubishi Corporation, offers Matlantis, a software-as-a-service platform that incorporates a product based on this research.

DATA AVAILABILITY

The data that support the findings of this article are not publicly available upon publication because it is not technically feasible and/or the cost of preparing, depositing, and hosting the data would be prohibitive within the terms of this research project. The data are available from the authors upon reasonable request.

[1] J. Hafner, *Ab-initio* simulations of materials using VASP: Density-functional theory and beyond, J. Comput. Chem. **29**, 2044 (2008).

[2] A. R. Oganov, *Modern Methods of Crystal Structure Prediction* (Wiley-VCH, Berlin, 2011).

[3] A. R. Oganov, C. J. Pickard, Q. Zhu, and R. J. Needs, Structure prediction drives materials discovery, Nat. Rev. Mater. **4**, 331 (2019).

[4] D. J. Wales, *Energy Landscapes Applications to Clusters, Biomolecules and Glasses* (Cambridge University Press, Cambridge, 2004).

[5] A. Jain, Y. Shin, and K. A. Persson, Computational predictions of energy materials using density functional theory, Nat. Rev. Mater. **1**, 15004 (2016).

[6] G. Hautier, C. Fischer, V. Ehrlacher, A. Jain, and G. Ceder, Data mined ionic substitutions for the discovery of new compounds, Inorg. Chem. **50**, 656 (2011).

[7] C. J. Pickard and R. J. Needs, *Ab initio* random structure searching, J. Phys.: Condens. Matter **23**, 053201 (2011).

[8] D. J. Wales and J. P. K. Doye, Global optimization by basin-hopping and the lowest energy structures of lennard-jones clusters containing up to 110 atoms, J. Phys. Chem. A **101**, 5111 (1997).

[9] M. Amsler and S. Goedecker, Crystal structure prediction using the minima hopping method, J. Chem. Phys. **133**, 224104 (2010).

[10] M. Krummenacher, M. Gubler, J. A. Finkler, H. Huber, M. Sommer-Jörgensen, and S. Goedecker, Performing highly efficient minima hopping structure predictions using the atomic simulation environment (ASE), SoftwareX **25**, 101632 (2024).

[11] D. M. Deaven and K. M. Ho, Molecular geometry optimization with a genetic algorithm, Phys. Rev. Lett. **75**, 288 (1995).

[12] A. R. Oganov and C. W. Glass, Crystal structure prediction using *ab initio* evolutionary techniques: Principles and applications, J. Chem. Phys. **124**, 244704 (2006).

[13] C. W. Glass, A. R. Oganov, and N. Hansen, USPEX—Evolutionary crystal structure prediction, Comput. Phys. Commun. **175**, 713 (2006).

[14] A. R. Oganov, A. O. Lyakhov, and M. Valle, How evolutionary crystal structure prediction works—and why, Acc. Chem. Res. **44**, 227 (2011).

[15] A. O. Lyakhov, A. R. Oganov, H. T. Stokes, and Q. Zhu, New developments in evolutionary structure prediction algorithm USPEX, Comput. Phys. Commun. **184**, 1172 (2013).

[16] D. C. Lonie and E. Zurek, XtalOpt: An open-source evolutionary algorithm for crystal structure prediction, Comput. Phys. Commun. **182**, 372 (2011).

[17] Z. Falls, P. Avery, X. Wang, K. P. Hilleke, and E. Zurek, The XtalOpt evolutionary algorithm for crystal structure prediction, J. Phys. Chem. C **125**, 1601 (2021).

[18] Y. Wang, J. Lv, L. Zhu, and Y. Ma, Crystal structure prediction via particle-swarm optimization, Phys. Rev. B **82**, 094116 (2010).

[19] T. Yamashita, N. Sato, H. Kino, T. Miyake, K. Tsuda, and T. Oguchi, Crystal structure prediction accelerated by Bayesian optimization, Phys. Rev. Mater. **2**, 013803 (2018).

[20] M. K. Bisbo and B. Hammer, Efficient global structure optimization with a machine-learned surrogate model, Phys. Rev. Lett. **124**, 086102 (2020).

[21] J. Behler and M. Parrinello, Generalized neural-network representation of high-dimensional potential-energy surfaces, Phys. Rev. Lett. **98**, 146401 (2007).

[22] A. P. Bartók, M. C. Payne, R. Kondor, and G. Csányi, Gaussian approximation potentials: the accuracy of quantum mechanics, without the electrons, Phys. Rev. Lett. **104**, 136403 (2010).

[23] A. V. Shapeev, Moment tensor potentials: a class of systematically improvable interatomic potentials, Multiscale Model. Simul. **14**, 1153 (2016).

[24] R. Drautz, Atomic cluster expansion for accurate and transferable interatomic potentials, Phys. Rev. B **99**, 014104 (2019).

[25] E. V. Podryabinkin, E. V. Tikhonov, A. V. Shapeev, and A. R. Oganov, Accelerating crystal structure prediction by machine-learning interatomic potentials with active learning, Phys. Rev. B **99**, 064114 (2019).

[26] C. Chen, W. Ye, Y. Zuo, C. Zheng, and S. P. Ong, Graph networks as a universal machine learning framework for molecules and crystals, Chem. Mat. **31**, 3564 (2019).

[27] C. Chen and S. P. Ong, A universal graph deep learning interatomic potential for the periodic table, Nat. Comput. Sci. **2**, 718 (2022).

[28] K. Choudhary, B. DeCost, L. Major, K. Butler, J. Thiyagalingam, and F. Tavazza, Unified graph neural network force-field for the periodic table: Solid state applications, Digit. Discov. **2**, 346 (2023).

[29] B. Deng, P. Zhong, K. Jun, J. Riebesell, K. Han, C. J. Bartel, and G. Ceder, CHGNet as a pretrained universal neural network potential for charge-informed atomistic modelling, Nat. Mach. Intell. **5**, 1031 (2023).

[30] I. Batatia, D. P. Kovacs, G. Simm, C. Ortner, and G. Csanyi, in *Advances in Neural Information Processing Systems*, Vol. 35, edited by S. Koyejo, S. Mohamed, A. Agarwal, D. Belgrave, K. Cho, and A. Oh (Curran Associates, Inc., 2022), pp. 11423–11436.

[31] I. Batatia, P. Benner, Y. Chiang, A. M. Elena, D. P. Kovács, J. Riebesell, X. R. Advincula, M. Asta, M. Avaylon, W. J. Baldwin, F. Berger, N. Bernstein, A. Bhowmik, F. Bigi, S. M. Blau, V. Cărare, M. Ceriotti, S. Chong, J. P. Darby, S. De, *et al.*, A foundation model for atomistic materials chemistry, J. Chem. Phys. **163**, 184110 (2025).

[32] A. Merchant, S. Batzner, S. S. Schoenholz, M. Aykol, G. Cheon, and E. D. Cubuk, Scaling deep learning for materials discovery, Nature (London) **624**, 80 (2023).

[33] M. Neumann, J. Gin, B. Rhodes, S. Bennett, Z. Li, H. Choubisa, A. Hussey, and J. Godwin, Orb: A fast, scalable neural network potential, arXiv:2410.22570.

[34] Y.-L. Liao, B. Wood, A. Das, and T. Smidt, in *International Conference on Learning Representations*, edited by B. Kim, Y. Yue, S. Chaudhuri, K. Fragki- adaki, M. Khan, and Y. Sun (2024) Vol. 2024, pp. 39282–39309.

[35] L. Barroso-Luque, S. Muhammed, X. Fu, B. Wood, M. Dzamba, M. Gao, A. Rizvi, C. L. Zitnick, and Z. W. Ulissi, Open materials 2024 (OMat24) inorganic materials dataset and models, arXiv:2410.12771.

[36] H. Yang, C. Hu, Y. Zhou, X. Liu, Y. Shi, J. Li, G. Li, Z. Chen, S. Chen, C. Zeni, M. Horton, R. Pinsler, A. Fowler, D. Zügner, T. Xie, J. Smith, L. Sun, Q. Wang, L. Kong, C. Liu, *et al.*, MatterSim: A deep learning atomistic model across elements, temperatures and pressures, arXiv:2405.04967.

[37] S. Takamoto, S. Izumi, and J. Li, TeaNet: Universal neural network interatomic potential inspired by iterative electronic relaxations, Comput. Mater. Sci. **207**, 111280 (2022).

[38] S. Takamoto, C. Shinagawa, D. Motoki, K. Nakago, W. Li, I. Kurata, T. Watanabe, Y. Yayama, H. Iriguchi, Y. Asano, T. Onodera, T. Ishii, T. Kudo, H. Ono, R. Sawada, R. Ishitani, M. Ong, T. Yamaguchi, T. Kataoka, A. Hayashi, *et al.*, Towards universal neural network potential for material discovery applicable to arbitrary combination of 45 elements, Nat. Commun. **13**, 2991 (2022).

[39] R. Jacobs, D. Morgan, S. Attarian, J. Meng, C. Shen, Z. Wu, C. Y. Xie, J. H. Yang, N. Artrith, B. Blaiszik, G. Ceder, K. Choudhary, G. Csanyi, E. D. Cubuk, B. Deng, R. Drautz, X. Fu, J. Godwin, V. Honavar, O. Isayev, *et al.*, A practical guide to machine learning interatomic potentials – Status and future, Curr. Opin. Solid State Mater. Sci. **35**, 101214 (2025).

[40] T. L. Jacobsen, M. S. Jørgensen, and B. Hammer, On-the-fly machine learning of atomic potential in density functional theory structure optimization, Phys. Rev. Lett. **120**, 026102 (2018).

[41] Q. Tong, L. Xue, J. Lv, Y. Wang, and Y. Ma, Accelerating CALYPSO structure prediction by data-driven learning of a potential energy surface, Faraday Discuss. **211**, 31 (2018).

[42] H. Wang, Y. Zhang, L. Zhang, and H. Wang, Crystal structure prediction of binary alloys via deep potential, Front. Chem. **8**, (2020).

[43] C. W. Park and C. Wolverton, Developing an improved crystal graph convolutional neural network framework for accelerated materials discovery, Phys. Rev. Mater. **4**, 063801 (2020).

[44] S. Kang, W. Jeong, C. Hong, S. Hwang, Y. Yoon, and S. Han, Accelerated identification of equilibrium structures of multicomponent inorganic crystals using machine learning potentials, npj Comput. Mater. **8**, 108 (2022).

[45] G. Cheng, X.-G. Gong, and W.-J. Yin, Crystal structure prediction by combining graph network and optimization algorithm, Nat. Commun. **13**, 1492 (2022).

[46] J. Schmidt, N. Hoffmann, H.-C. Wang, P. Borlido, P. J. M. A. Carriço, T. F. T. Cerqueira, S. Botti, and M. A. L. Marques, Machine-learning-assisted determination of the global zero-temperature phase diagram of materials, Adv. Mater. **35**, 2210788 (2023).

[47] L. Chang, H. Tamaki, T. Yokoyama, K. Wakasugi, S. Yotsuhashi, M. Kusaba, A. R. Oganov, and R. Yoshida, Downfolding from *ab initio* to interacting model Hamiltonians: comprehensive analysis and benchmarking of the DFT+cRPA approach, npj Comput. Mater. **10**, 129 (2024).

[48] S. Donaldson, R. A. Lawrence, and M. I. J. Probert, A genetic algorithm for convex hull optimisation, arXiv:2404.14354.

[49] P. E. Blöchl, Projector augmented-wave method, Phys. Rev. B **50**, 17953 (1994).

[50] G. Kresse and D. Joubert, From ultrasoft pseudopotentials to the projector augmented-wave method, Phys. Rev. B **59**, 1758 (1999).

[51] J. P. Perdew, K. Burke, and M. Ernzerhof, Generalized gradient approximation made simple, Phys. Rev. Lett. **77**, 3865 (1996).

[52] G. Kresse and J. Hafner, *Ab initio* molecular dynamics for liquid metals, Phys. Rev. B **47**, 558 (1993).

[53] G. Kresse and J. Furthmüller, Efficient iterative schemes for *ab initio* total-energy calculations using a plane-wave basis set, Phys. Rev. B **54**, 11169 (1996).

[54] G. Kresse and J. Furthmüller, Efficiency of *ab-initio* total energy calculations for metals and semiconductors using a plane-wave basis set, Comput. Mater. Sci. **6**, 15 (1996).

[55] S. L. Dudarev, G. A. Botton, S. Y. Savrasov, C. J. Humphreys, and A. P. Sutton, Electron-energy-loss spectra and the structural stability of nickel oxide: An LSDA+U study, Phys. Rev. B **57**, 1505 (1998).

[56] A. Jain, S. P. Ong, G. Hautier, W. Chen, W. D. Richards, S. Dacek, S. Cholia, D. Gunter, D. Skinner, G. Ceder, and K. A. Persson, Commentary: The Materials Project: A materials genome approach to accelerating materials innovation, APL Mater. **1**, 011002 (2013).

[57] L. Wang, T. Maxisch, and G. Ceder, Oxidation energies of transition metal oxides within the GGA + U framework, Phys. Rev. B **73**, 195107 (2006).

[58] M. J. Mehl, D. Hicks, C. Toher, O. Levy, R. M. Hanson, G. Hart, and S. Curtarolo, The AFLOW library of crystallographic prototypes: part 1, Comput. Mater. Sci. **136**, S1 (2017).

[59] S. P. Ong, W. D. Richards, A. Jain, G. Hautier, M. Kocher, S. Cholia, D. Gunter, V. L. Chevrier, K. A. Persson, and G. Ceder, Python Materials Genomics (pymatgen): A robust, open-source python library for materials analysis, Comput. Mater. Sci. **68**, 314 (2013).

[60] A. Wang, R. Kingsbury, M. McDermott, M. Horton, A. Jain, S. P. Ong, S. Dwaraknath, and K. A. Persson, A framework for quantifying uncertainty in DFT energy corrections, Sci. Rep. **11**, 15496 (2021).

[61] A. Jain, G. Hautier, S. P. Ong, C. J. Moore, C. C. Fischer, K. A. Persson, and G. Ceder, Formation enthalpies by mixing GGA and GGA + *U* calculations, Phys. Rev. B **84**, 045115 (2011).

[62] G. Trimarchi, A. J. Freeman, and A. Zunger, Predicting stable stoichiometries of compounds via evolutionary global space-group optimization, Phys. Rev. B **80**, 092101 (2009).

[63] C. J. Bartel, Review of computational approaches to predict the thermodynamic stability of inorganic solids, J. Mater. Sci. **57**, 10475 (2022).

[64] S. S. Omee, L. Wei, M. Hu, and J. Hu, Crystal structure prediction using neural network potential and age-fitness Pareto genetic algorithm, J. Mater. Inform. **4**, (2024).

[65] S. S. Omee, L. Wei, S. Dey, and J. Hu, Polymorphism crystal structure prediction with adaptive space group diversity control, Adv. Sci. **12**, e10792 (2025).

[66] D. E. Goldberg, J. Richardson, *et al.*, in *Genetic Algorithms and their Applications: Proceedings of the Second International*

Conference on Genetic Algorithms, Vol. 4149 (Lawrence Erlbaum, Hillsdale, NJ, 1987), pp. 414–425.

[67] K. Deb, A. Pratap, S. Agarwal, and T. Meyarivan, A fast and elitist multiobjective genetic algorithm: NSGA-II, IEEE Trans. Evol. Comput. **6**, 182 (2002).

[68] K. Deb and H. Jain, An evolutionary many-objective optimization algorithm using reference-point-based nondominated sorting approach, part i: Solving problems with box constraints, IEEE Trans. Evol. Comput. **18**, 577 (2014).

[69] T. Akiba, S. Sano, T. Yanase, T. Ohta, and M. Koyama, in *Proceedings of the 25th ACM SIGKDD International Conference on Knowledge Discovery & Data Mining* (Association for Computing Machinery, New York, 2019), pp. 2623–2631.

[70] A. H. Larsen, J. J. Mortensen, J. Blomqvist, I. E. Castelli, R. Christensen, M. Dułak, J. Friis, M. N. Groves, B. Hammer, C. Hargus, E. D. Hermes, P. C. Jennings, P. B. Jensen, J. Kermode, J. R. Kitchin, E. L. Kolsbjerg, J. Kubal, K. Kaasbjerg, S. Lysgaard, J. B. Maronsson, *et al.*, The atomic simulation environment—a Python library for working with atoms, J. Phys. Condens. Matter **29**, 273002 (2017).

[71] A. O. Lyakhov, A. R. Oganov, and M. Valle, How to predict very large and complex crystal structures, Comput. Phys. Commun. **181**, 1623 (2010).

[72] S. Fredericks, K. Parrish, D. Sayre, and Q. Zhu, PyXtal: A Python library for crystal structure generation and symmetry analysis, Comput. Phys. Commun. **261**, 107810 (2021).

[73] N. L. Abraham and M. I. J. Probert, Improved real-space genetic algorithm for crystal structure and polymorph prediction, Phys. Rev. B **77**, 134117 (2008).

[74] M. Valle and A. R. Oganov, in *2008 IEEE Symposium on Visual Analytics Science and Technology* (IEEE, 2008), pp. 11–18.

[75] A. R. Oganov and M. Valle, How to quantify energy landscapes of solids, J. Chem. Phys. **130**, 104504 (2009).

[76] A. R. Oganov, Y. Ma, A. O. Lyakhov, M. Valle, and C. Gatti, Evolutionary crystal structure prediction as a method for the discovery of minerals and materials, Rev. Mineral. Geochem. **71**, 271 (2010).

[77] Q. Zhu, A. R. Oganov, and A. O. Lyakhov, Evolutionary metadynamics: A novel method to predict crystal structures, CrystEngComm **14**, 3596 (2012).

[78] E. Real, A. Aggarwal, Y. Huang, and Q. V. Le, in *in Proceedings of the Thirty-Third AAAI Conference on Ar- tificial Intelligence and Thirty-First Innovative Appli- cations of Artificial Intelligence Conference and Ninth AAAI Symposium on Educational Advances in Artificial Intelligence* (AAAI Press, Honolulu, 2019).

[79] The modified crossover and mutation methods are released and available at https://pypi.org/project/pfn-ase-extras/.

[80] L. B. Vilhelmsen and B. Hammer, Systematic study of Au_6 to Au_{12} gold clusters on MgO(100) *F* centers using density-functional theory, Phys. Rev. Lett. **108**, 126101 (2012).

[81] P. J. Clark and F. C. Evans, Distance to nearest neighbor as a measure of spatial relationships in populations, Ecology **35**, 445 (1954).

[82] C. Zeni, R. Pinsler, D. Zügner, A. Fowler, M. Horton, X. Fu, Z. Wang, A. Shysheya, J. Crabbé, S. Ueda, R. Sordillo, L. Sun, J. Smith, B. Nguyen, H. Schulz, S. Lewis, C.-W. Huang, Z. Lu, Y. Zhou, H. Yang, *et al.*, A generative model for inorganic materials design, Nature (London) **639**, 624 (2025).

[83] See Supplemental Material at http://link.aps.org/supplemental/10.1103/4knt-ccqg for crystal structures in *xyz* formats.

[84] A. Togo, K. Shinohara, and T. Isao, Spglib a software library for crystal symmetry search, Sci. Technol. Adv. Mater., Meth. **4**, 2384822 (2024).

[85] D. Hicks, M. J. Mehl, E. Gossett, C. Toher, O. Levy, R. M. Hanson, G. Hart, and S. Curtarolo, The AFLOW library of crystallographic prototypes: Part 2, Comput. Mater. Sci. **161**, S1 (2019).

[86] D. Hicks, M. J. Mehl, M. Esters, C. Oses, O. Levy, G. L. Hart, C. Toher, and S. Curtarolo, The AFLOW library of crystallographic prototypes: Part 3, Comput. Mater. Sci. **199**, 110450 (2021).

[87] H. Eckert, S. Divilov, M. J. Mehl, D. Hicks, A. C. Zettel, M. Esters, X. Campilongo, and S. Curtarolo, The AFLOW library of crystallographic prototypes: Part 4, Comput. Mater. Sci. **240**, 112988 (2024).

[88] R. E. Goodall, A. S. Parackal, F. A. Faber, R. Armiento, and A. A. Lee, Rapid discovery of stable materials by coordinate-free coarse graining, Sci. Adv. **8**, eabn4117 (2022).